Raindrop Detection on Car Windshields Using Geometric-Photometric Environment Construction and Intensity-Based Correlation

Jad C. Halimeh and Martin Roser
Institut für Mess- und Regelungstechnik
Universität Karlsruhe (TH)
D-76131 Karlsruhe, Germany
Email: jad.halimeh@stud.uni-karlsruhe.de, roser@mrt.uka.de

***Abstract*— Vision-based Driver Assistance Systems (DAS) are becoming pervasive in today's automotive industry. However, most of these systems are designed to perform in good weather conditions and they perform very poorly in adverse weather particularly in rain. A big problem related to rainy weather conditions that highly limits the performance of DAS is raindrops on car windshields. We present a novel approach that detects raindrops on a car windshield using only a single image from an in-vehicle camera and a standard interest point detector for pre-selection of raindrop candidates. The algorithm models the geometric shape of a raindrop on the car windshield, utilizes its photometric properties and establishes a relationship between raindrop and environment. The proposed algorithm outperforms existing machine vision-based approaches for the task of raindrop modeling and detection from an in-vehicle perspective. It functions very accurately and is robust in terms of imprecise positions of raindrop candidates. Its results can be further used for image restoration and vision enhancement and hence it is a valuable tool for DAS.**

I. INTRODUCTION

Vision-based Driver Assistance Systems (DAS) are becoming pervasive in today's automotive industry. They provide assistance to the driver in multiple ways and drastically minimize the risk of accidents. Since most weather-related accidents arise due to rainy weather conditions, reliable assistance in such situations is desirable. However, DAS are designed to perform under good-natured weather conditions and are heavily affected in adverse weather, especially in rain. This means the driver has to live with limited DAS functionality particularly in such situations where assistance and guidance are most desired. Therefore, a reliable raindrop detection system is needed that provides proper compensation for the shortcomings of today's vision sensors in rainy weather by providing additional information like raindrop position and size. These parameters can then be used to enhance image processing algorithms for DAS and are an important step towards extending their functionality to adverse weather conditions.

Bad weather conditions can be classified into two main categories: Static or steady weather conditions such as fog, mist, or haze and dynamic weather conditions such as rain, hail, or snow. Whereas many attempts have been made at resolving static weather problems like fog or haze [12], [15], [13], [8], research in machine vision for dynamic weather conditions is sparse.

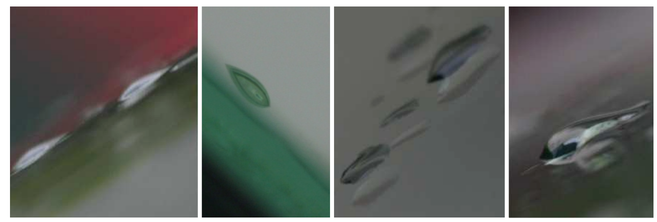

Fig. 1. Shapes of raindrops on windshields

Garg and Nayar [4], [5], [6], [7] studied the visual effects of rain and came up with a photometric raindrop model that describes refraction and reflection of light by a stationary, spherical raindrop. Additionally, they determined the effect of camera parameters on image disturbance and developed an approach of detecting and removing rain from videos. Zhang *et al.* [17] further extended the rain detection approach in [4] by chromatic properties. However, these approaches require simplifications, *e.g.* a static observer or high exposure time and hence are not efficient in in-vehicle applications with egomotion. In addition, rain streaks as discussed by Garg and Nayar are not the dominant weather feature in the application discussed in this paper, but rather the main feature here are raindrops on the car windshield.

Kurihata [11] used a machine learning approach with raindrop templates, so called *eigendrops*, to detect raindrops on windshields. Results within the sky area were quite promising, whereas the proposed method produced a large number of false positives within the non-sky regions of the image where background texture and raindrop appearance get sophisticated.

Raindrop modeling was also performed using ray tracing [14], [2]. Unfortunately, ray tracing algorithms are computationally very expensive. Cameron *et al.* [2] proposed an approach that uses multiple DSPs in order to reduce the processing time, but their approach still does not offer itself to real-time applications. A real-time approach was proposed in [14] that employed two models, the physical model that described the water movement, followed by a lighting model that took Fresnel's reflectivity coefficients into account. However, their goal was not to create a physically correct model but rather a credible simulation for computer graphics applications. The main goal of the approach discussed in this paper is the physically accurate modeling of raindrops on a tilted glass surface so that real raindrops can be detected and distinguished from non-raindrop blobs.

This paper introduces an algorithm based on a novel geometric-photometric model that thoroughly describes the refractive properties of a raindrop on a car windshield. The algorithm traces the rays going through this raindrop from the environment into the camera, and determines the part of the scene refracted by the raindrop. Fresnel's reflectivity coefficients are then used to perform intensity-based correlation between the raindrop and the section of the environment (scene) it refracts to verify that it is a raindrop. The algorithm we have developed and tested is coined the *Raindrop Intelligent Geometric Scanner and Environment Constructor (RIGSEC)*. The original image location and radius of the blob initially assumed to be a raindrop are attained using a Hessian-based interest point detector such as SURF [1]. Those are then input into RIGSEC and the latter determines if that blob in the image is the result of a raindrop on the windshield.

II. GEOMETRIC-PHOTOMETRIC RAINDROP MODEL

A standard detector provides n possible raindrop candidates with position $\mathbf{x}_i = (x_i, y_i)^T$ and radius r_i ($i = 1..n$) in the image plane, so the sensed raindrop candidate can be described completely by $\mathbf{p}_i = (x_i, y_i, r_i)^T$. Based on these detection results, each candidate is tested with RIGSEC. The algorithm is explained in the following taking into account only one possible raindrop candidate $\mathbf{p} = (x, y, r)^T$.

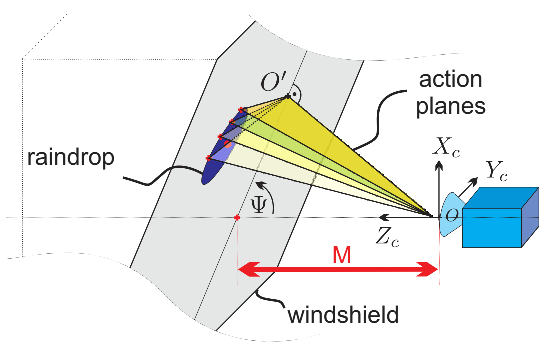

Fig. 2. Geometric framework of proposed method with action planes

A 3D camera coordinate system $\mathbf{X} = (X_C, Y_C, Z_C)^T$ is built as shown in Fig. 2 with its origin lying at the camera optical center O. The optical axis makes an angle Ψ with the inner windshield plane W_i and intersects it at a distance M. The optical center O, its orthogonal projection O' on W_i, and each scanned point on the detected blob form an *action plane*, with the major action plane (defined by the points O, O', and the raindrop center on W_i) being of particular interest. Such a plane is called an action plane because, according to Snell's law of refraction [9], the light ray passing through the corresponding scanned point to the optical center never leaves this plane ever since coming from the raindrop surface. Thus, the light ray is always in this plane but not necessarily so before it reaches the raindrop.

Fig. 3 shows a detailed view on one action plane. The windshield of thickness T is modeled as two parallel planes W_i (inner plane) and W_o (outer plane). Hence, the orthogonal projections on W_i and W_o are given respectively by

$$\mathbf{O}' = M \sin \Psi \hat{\mathbf{n}}_W \tag{1}$$

$$\mathbf{O}'' = \mathbf{O}' + T\hat{\mathbf{n}}_W = (M \sin \Psi + T)\hat{\mathbf{n}}_W \tag{2}$$

where $\hat{\mathbf{n}}_W = (\cos \Psi, 0, \sin \Psi)^T$ is the windshield normal. The real-world coordinates $\mathbf{X}_i$ of $\mathbf{p}$ on W_i can then be determined using the pinhole camera model and the focal length f:

$$X_i = Z_i \frac{x}{f} \tag{3}$$

$$Y_i = Z_i \frac{y}{f} \tag{4}$$

$$Z_i = \frac{M tan\Psi}{tan\Psi + \frac{x}{f}} \tag{5}$$

Accordingly, the corresponding raindrop radius on W_i is

$$R_i = Z_i \frac{r}{f}. \tag{6}$$

Due to glass refraction effects, the raindrop position on W_o slightly varies and its radius R_i is actually larger than it appears on W_i. Hence, in order to determine the actual position $\mathbf{X}_o$ and size R_o of the sensed raindrop on W_o, the raindrop extremities (see Fig. 3) are traced from W_i to their counterparts on W_o. All other rays in between the extremities can be traced using Snell's law of refraction as follows: Consider any given ray $\mathbf{S} = \vec{OS} = (X_S, Y_S, Z_S)^T$ on W_i as depicted in Fig. 3 (dashed line). The angle of incidence α of vector $\mathbf{S}$ with respect to the windshield normal is then given by

$$\alpha = \arccos \left(\frac{\mathbf{S} \cdot \hat{\mathbf{n}}_W}{||\mathbf{S}||} \right). \tag{7}$$

The *piercing point* R of the ray with W_o can be determined using Snell's law, refraction indices of air and glass and (1):

$$\kappa = \arcsin \left(\frac{n_{\text{air}} \sin \alpha}{n_{\text{glass}}} \right) \tag{8}$$

$$\mathbf{R} = \mathbf{S} + T \left(\hat{\mathbf{n}}_W + \frac{\tan \kappa}{||\mathbf{SO}'||} (\mathbf{S} - M \sin \Psi \hat{\mathbf{n}}_W) \right). \tag{9}$$

This means that for any point on the raindrop whose image coordinates are known, its XYZ-coordinates on W_o can be determined. The above equations also provide the XYZ-coordinates of the interface extremities on W_o since the corresponding coordinates of the blob extremities on W_i are known. The real blob radius R_o and its center position C_o on W_o can then be determined.

The shape of fluid droplets on solid surfaces is modeled using the Young-Laplace equation [16], [3] that describes the relation between surface tension, pressure and curvature. The

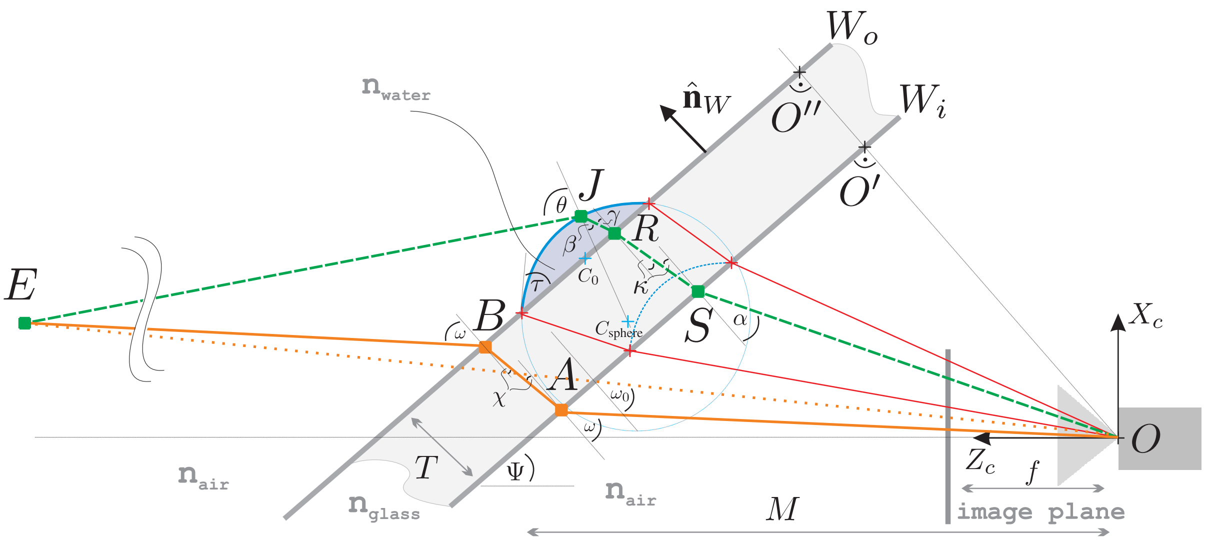

Fig. 3. Refraction model for an example action plane

contact angle τ between the raindrop surface and W_o plays the role of a boundary condition. In addition to the above relations, the exact contact angle depends on the treatment of the solid surface as well as the rain water consistency. Typical values are approximately $30^\circ - 50^\circ$. For simplicity, the raindrop is considered to be a spherical section with cut surface radius R_o on W_o and contact angle τ between the raindrop surface and W_o. This leads to determining the *extended* sphere:

$$R_{\text{sphere}} = \frac{R_o}{\sin\tau} \tag{10}$$

$$\mathbf{C}_{\text{sphere}} = \mathbf{C}_o - \hat{\mathbf{n}}_W R_{\text{sphere}} \cos\tau. \tag{11}$$

Considering the dashed ray from Fig. 3, point J on the drop surface can be determined as the piercing point of the ray coming back from S and being refracted at R towards $\hat{\mathbf{n}}_W$ according to the refractive indices n_{glass} and n_{water}

$$\gamma = \arcsin\left(\frac{n_{\text{glass}} \sin\kappa}{n_{\text{water}}}\right). \tag{12}$$

The angle of incidence at the raindrop surface is particularly important for identifying refracted environment areas. The angle of refraction at point J is given by

$$\beta = \arccos\left(\frac{\hat{\mathbf{n}}_{\text{sphere}}(\mathbf{J}) \cdot \mathbf{RJ}}{||\mathbf{RJ}||}\right) \tag{13}$$

where the raindrop surface normal $\hat{\mathbf{n}}_{\text{sphere}}(J)$ is now dependent on the surface point J. Hence, the ray leaves the action plane from Fig. 3 and propagates in a plane formed by R, J and C_{sphere} as depicted in Fig. 4.

The angle of incidence θ at point J can be determined in line with (12) but with β, n_{water} and n_{air}:

$$\theta = \arcsin\left(\frac{n_{\text{water}} \sin\beta}{n_{\text{air}}}\right) \tag{14}$$

In case that no total internal reflection occurs inside the raindrop at J, RIGSEC determines the point E in the environment from which this light ray emanates, assuming E lies on a known environment plane. Even though RIGSEC works for any geometrical surface in the environment, a plane with the equation $\hat{\mathbf{n}}_{\text{env}} \cdot \mathbf{X} + d = 0$ is taken to be the environment for simplicity.

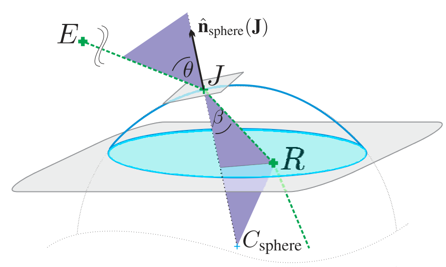

Fig. 4. Plane of light ray coming from environment and incident at raindrop surface point J

In order to decide on the raindrop candidate, the 3D environment point E has to be traced to an observation at position $\mathbf{x}$ in the image plane, denoted by the light ray going from E to O by propagating through air into the windshield glass and finally into the inside of the vehicle towards O. The light ray is incident to W_o at an angle ω and leaves W_i making also an angle of ω with the opposite of $\hat{\mathbf{n}}_W$. The dotted line EO makes an angle ω_0 with $\hat{\mathbf{n}}_W$ which is calculated to be

$$\omega_0 = \arccos\left(\frac{\mathbf{OE} \cdot \hat{\mathbf{n}}_W}{||\mathbf{OE}||}\right). \tag{15}$$

Note that the points E, B, A, O, O', and O'' are all in the same action plane. Finding ω results in a nonlinear problem which can be solved by standard techniques like the Newton-Raphson method that iteratively solves the root problem $f(\omega) = (\cot(\omega + \Psi_P), -1) \cdot (\mathbf{x}_E^* - \mathbf{x}_B^*) = 0$, starting with the initial angle ω_0. $\mathbf{x}_E^*$, $\mathbf{x}_B^*$, and Ψ_P are the projection of E, B, and Ψ, on the action plane mentioned above.

III. INTENSITY-BASED CORRELATION

Based on the sensed location of a blob, RIGSEC determines the exact path of all light rays that are interacting with the raindrop starting in the image plane and tracing them back to the environment where they emanate. However, in order to compare the environment mapped to the raindrop candidate, predicting the observed pixel intensity is at least as essential as the exact ray tracing discussed above. Hence, RIGSEC uses the environment intensities and Fresnel's reflectivity coefficients.

When light moves from a medium of a given refractive index n_1 into a second medium with refractive index n_2, both reflection and refraction of light may occur. Since in this application only the refracted part accounts for the light that reaches the optical center due to the geometry of the raindrops on a car windshield, the transmitted light intensity I_2 will be related to the incident light intensity I_1 by

$$I_2 = (1 - R_{12}) I_1 \tag{16}$$

where R_{12} is Fresnel's reflectivity coefficient for sunlight in the atmosphere going from medium 1 to medium 2. Even though unpolarized in space, sunlight becomes partially polarized in the atmosphere due to scattering from gas molecules and reflection off objects according to [9]. However, much of the light impinging on the camera is only slightly polarized, and totally polarized light occurs only at a few specific angles (*e.g.* Brewster angle in case of reflection). Hence, it can be assumed over time average that the light has an approximately equal mix of parallel and perpendicular polarizations and R_{12} can be expressed as

$$R_{12} = \frac{1}{2}\left(r^2_{12_\parallel} + r^2_{12_\perp}\right) \tag{17}$$

where according to [10]

$$r_{12_\perp} = \frac{n_1 \cos\mu_1 - n_2 \cos\mu_2}{n_1 \cos\mu_1 + n_2 \cos\mu_2} \tag{18}$$

$$r_{12_\parallel} = \frac{n_1 \cos\mu_2 - n_2 \cos\mu_1}{n_1 \cos\mu_2 + n_2 \cos\mu_1} \tag{19}$$

The corresponding values for μ_1, μ_2, n_1, and n_2 can be found in Table I. Since I_A is known from the camera, this intensity is transmitted by the light ray going from E to the optical center via raindrop and glass refraction. The estimated raindrop intensity $\hat{I}_S$ at S can be determined as

$$\hat{I}_S = \frac{I_A}{\prod_i (1 - R_i)^j} \tag{20}$$

where R_i are Fresnel's reflectivity coefficients at all points where refraction between two media occurs (*i.e.* $i \in \{A, B, J, R, S\}$, see Fig. 3) and j stands for the direction of the intensity prediction:

$$j = \begin{cases} -1, & \forall i \in \{A, B\} \\ 1, & \text{else} \end{cases} \tag{21}$$

Table I shows all relevant information for estimating $\hat{I}_S$:

TABLE I

PARAMETERS FOR FRESNEL'S REFLECTIVITY COEFFICIENTS

point	transition	n_1	n_2	μ_1	μ_2
A	air/glass	n_{air}	n_{glass}	ω	χ
B	glass/air	n_{glass}	n_{air}	χ	ω
J	air/water	n_{air}	n_{water}	θ	β
R	water/glass	n_{water}	n_{glass}	γ	κ
S	glass/air	n_{glass}	n_{air}	κ	α

IV. EXPERIMENTS

As depicted in Fig. 5, the experimental setup consists of a windshield plane and an environment plane that can both be tilted at different angles and translated along the optical axis of the camera. Furthermore, one artificial pattern and one image of a real traffic scene were used as experimental environments where, for purpose of simplicity, the real traffic scene was assumed to be planar as well.

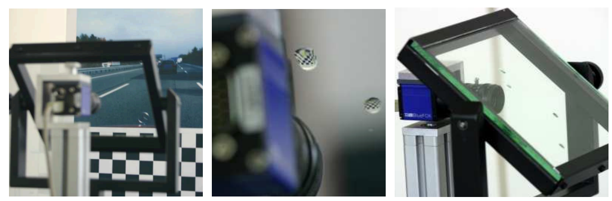

Fig. 5. Experimental setup for RIGSEC

In order to reach a decision about the raindrop candidate, the error between observed pixel intensities I_S and estimated intensities $\hat{I}_S$ is evaluated using the correlation coefficient

$$\text{CC} = \frac{1}{N\sigma_{\hat{I}}\sigma_I}\sum_{i=1}^{N}(\hat{I}_i - \overline{\hat{I}})(I_i - \overline{I}) \tag{22}$$

with mean values and standard deviations $\overline{I}, \sigma_I$ for the observed values and $\overline{\hat{I}}, \sigma_{\hat{I}}$ for the estimated values, respectively, and with N as the number of all estimates.

V. RESULTS

Experiments reveal that for both environments accurate construction is achieved. Fig. 6 shows scanned raindrops with the scenes they refract as observed by the camera (upper rows) and as constructed by RIGSEC (lower rows) for the two above-mentioned environments. The CC values in Fig. 6 show the correlation coefficient between construction and observation. MaxCorr takes the maximum of CC in a small ROI around the raindrop position estimate.

Although the visual results are quite accurate and correlation coefficients up to 0.74 are achieved, correlation especially for the artificial pattern is less significant. As an example, the three top-left raindrops in Fig. 6 show only low correlation (CC $= 0.08, 0.13, 0.05$) even though the algorithm yields accurate geometric environment contruction. This can be explained due to the following reasons: Firstly, a raindrop can be assumed as an additional lens on the windshield so light rays from a pixel diverge and each observed point (pixel) on the raindrop integrates the light

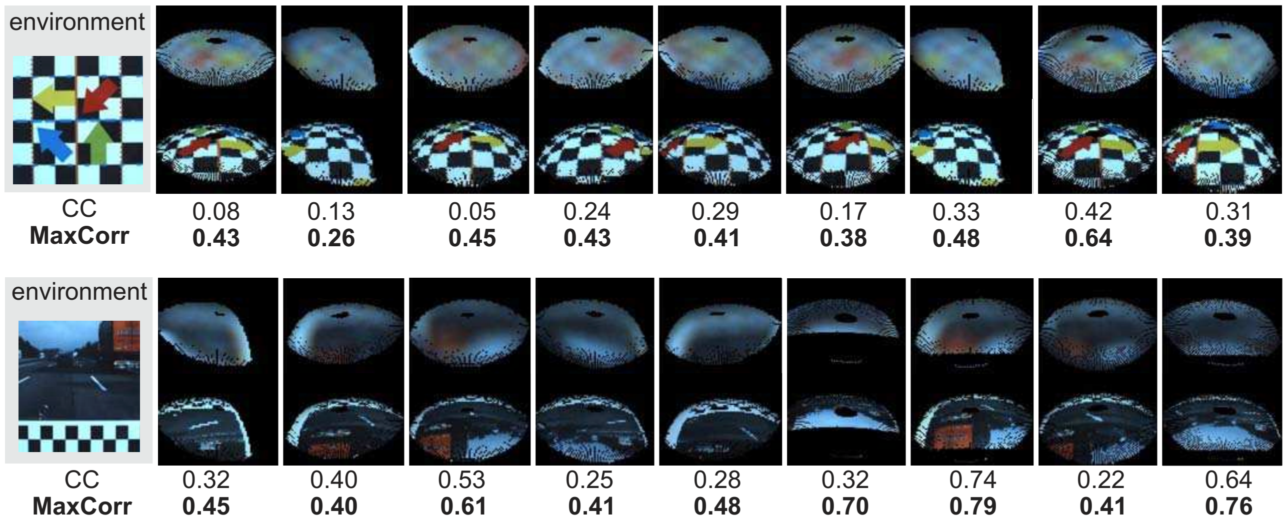

Fig. 6. Upper images show the real raindrop (observation), lower images show RIGSEC construction results. Black area within a raindrop indicates the refracted environment area occluded by the raindrop. Black areas along the boundary of a raindrop are refracted scene patches not subtended in the field of view of the DAS camera. Both types of areas are omitted from the process of intensity correlation due to the fact that no information on their intensities is readily available. The black dots around the boundary of the raindrop are due to finite scanning resolution.

of an environmental area of many pixels in size. Secondly, the raindrop appears blurred since the camera focuses near infinity.

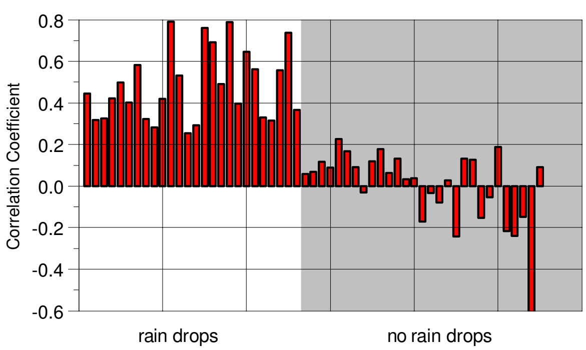

Fig. 7. Correlation coefficient for true positives and false positives

However, the goal was to develop a physically correct model for relating the environment to the observed raindrop candidate and getting accurate construction rather than adapting the construction results to the undersampled, out-of-focus raindrop observation. Due to the large number of raindrops falling on the windshield, a 100% classification is not needed. Thus, incorporating these steps is not neccessary for this paper but will be future work for improving the application of RIGSEC. As depicted in Fig. 7, the correlation coefficient is already distinct enough to decide on a raindrop candidate.

The task of raindrop detection from an in-vehicle camera is characterized by a disadvantegeous camera mounting position very close to the highly tilted windshield and a strong curvature of the refractive raindrop surface. Even small changes in the initial raindrop candidate position can lead to less than optimal correlation results when RIGSEC is run only once. This makes the algorithm highly dependent on the initial positions of raindrop candidates. Since the position results of common regional descriptors like SURF are not very accurate for raindrops, robustness to imprecise initial positions has to be improved. Simulations reveal that for small changes in position, the gradient of the drop surface as well as Snell's law can be linearized. It can be assumed that the RIGSEC result itself does not change much except for a linear translation of the geometrically constructed environment area. Hence, RIGSEC need not be performed again. Matching the previous result within a small ROI would be sufficient to find the optimized raindrop position.

In order to verify that assumption, RIGSEC is performed for a varying set of raindrop positions as depicted in Fig. 8(a). Fig. 8(b) shows high sensitivity of the correlation results to these imprecise initial positions. However, after maximizing the CC values of each RIGSEC run by matching the constructed environment within a small ROI, the raindrop positions converge to the optimum (8(c)). As shown in Fig. 8(b) all CC values also converge to MaxCorr, which is a robust correlation measure even for imprecise positions of raindrop candidates.

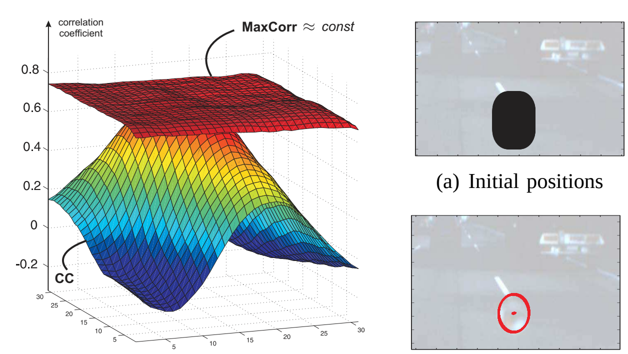

(a) Initial positions

(b) CC for initial position (curved) and optimized position (red plane)

(c) Optimized positions

Fig. 8. Robustness of RIGSEC with regards to inaccurate initial positions

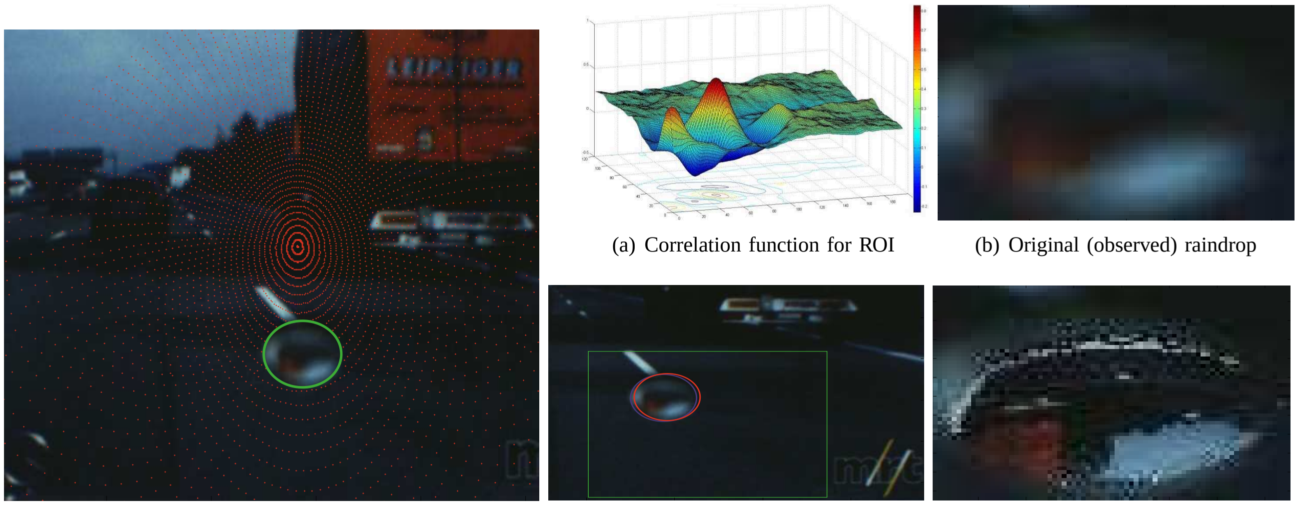

(a) Correlation function for ROI

(b) Original (observed) raindrop

(c) Determination of environment points

(d) ROI for raindrop matching

(e) Constructed raindrop

Fig. 9. Results of proposed algorithm. (b) shows the observed raindrop. In (c), RIGSEC determines the environment mapped by the blob had it been a raindrop. (d) Matching the construction results leads to the exact raindrop position deduced from (a). For demonstration purposes, the scene is constructed and placed at the raindrop position as shown in (e).

Fig. 9(d) shows the RIGSEC geometric scanning results for a (mislocated) raindrop candidate after a single run of the algorithm. The constructed raindrop is then matched within a small ROI as depicted in Fig. 9(b). It can be clearly seen that the correlation function reaches its global maximum at the precise raindrop position (Fig. 9(c)).

VI. CONCLUSIONS AND FUTURE WORK

A geometric and photometric approach was proposed for the determination of the environmental area refracted by a raindrop on a car windshield. Intensity-based correlation was then used for a reliable decision on the raindrop candidate. It could be shown that our algorithm performs very accurately and is robust in terms of imprecise initial positions which makes it applicable even in combination with standard interest point detectors that only provide inaccurate raindrop candidate positions.

Future work includes reducing computational time for the development of a real time add-in for DAS. In order to emphasize the strength of our algorithm and to get a precise quantitative measure for raindrop correlation, an exact out-of-focus blurring function as well as the determination of environmental areas are necessary as discussed in Section V and are in the works.

VII. ACKNOWLEDGMENTS

This work is partly supported by Honda R&D Europe. The authors would also like to thank the Karlsruhe School of Optics and Photonics (KSOP) of the University Karlsruhe.

REFERENCES

[1] Herbert Bay, Tinne Tuytelaars, and Luc Van Gool. *Lecture Notes in Computer Science*, volume 3951/2006, chapter SURF: Speeded Up Robust Features, pages 404–417. Springer Berlin / Heidelberg, 2006.

[2] C.B. Cameron, R.N. Rodriguez, N. Padgett, E. Waluschka, S. Kizhner, G. Colon, and C. Weeks. Fast optical ray tracing using multiple dsps. volume 55, pages 801–808, 2006.

[3] Roland Clift, John R. Grace, and Martin E. Weber. *Bubbles, drops, and particles*. Acad. Pr., 1978.

[4] K. Garg and S.K. Nayar. Detection and removal of rain from videos. In *IEEE Conference on Computer Vision and Pattern Recognition (CVPR)*, volume I, pages 528–535, Jun 2004.

[5] K. Garg and S.K. Nayar. When does a camera see rain? In *IEEE International Conference on Computer Vision (ICCV)*, volume 2, pages 1067–1074, Oct 2005.

[6] K. Garg and S.K. Nayar. Photorealistic rendering of rain streaks. *ACM Trans. on Graphics (also Proc. of ACM SIGGRAPH)*, Jul 2006.

[7] K. Garg and S.K. Nayar. Vision and rain. *Internatl. Journal of Computer Vision*, 75(1):3–27, 2007.

[8] Nicolas Hautière, Jean-Philippe Tarel, and Didier Aubert. Simultaneous contrast restoration and obstacles detection: First results. In *IEEE Intelligent Vehicle Symposium (IV'2007)*, pages 130–135, Istanbul, Turkey, 2007. http://perso.lcpc.fr/tarel.jean-philippe/iv07.html.

[9] Eugene Hecht. *Optics*. Reading, Mass. : Addison-Wesley Pub. Co., 4. ed. edition, 2002.

[10] Claus Klingshirn. *Semiconductor Optics*. Springer, 3. ed. edition, 2007.

[11] H. Kurihata, T. Takahashi, I. Ide, Y. Mekade, H. Muraseand Y. Tamatsu, and T. Miyahara. Rainy weather recognition from in-vehicle camera images for driver assistance. In *IEEE Intelligent Vehicles Symposium*, pages 205–210, 2005.

[12] S.G. Narasimhan and S.K. Nayar. Vision and the atmosphere. *Internatl. Journal of Computer Vision*, 48(3):233–254, 2002.

[13] Dean Pomerleau. Visibility estimation from a moving vehicle using the ralph vision system. In *IEEE Conference on Intelligent Transportation Systems*, pages 906 – 911, November 1997.

[14] I. Stuppacher and P. Supan. Rendering of water drops in real-time. In *Central European Seminar on Computer Graphics for students (CESCG 2007)*, 2007.

[15] R. Tan, N. Pettersson, and L. Petersson. Visibility enhancement for roads with foggy or hazy scenes. In *IEEE Intelligent Vehicle Symposium (IV'2007)*, pages 19–24, Istanbul, Turkey, 2007.

[16] K. L. Wolf. *Physik der Grenzflächen - Die Phänomene im Allgemeinen*. Springer, 1957.

[17] Xiaopeng Zhang, Hao Li, Yingyi Qi, Wee Kheng Leow, and Teck Khim Ng. Rain removal in video by combining temporal and chromatic properties. pages 461–464, 2006.